Deep eutectic solvents interaction with asphaltenes

A combined experimental and molecular dynamics study

Hebbar, Akshatha; Debraj, Devangshi; Acharya, Sriprasad; Puttapati, Sampath Kumar; Vatti, Anoop Kishore; Dey, Poulumi

DOI
10.1016/j.molliq.2023.122627

Publication date
2023

Document Version
Final published version

Published in
Journal of Molecular Liquids

Journal of Molecular Liquids 387 (2023) 122627

Contents lists available at ScienceDirect

Journal of Molecular Liquids

journal homepage: www.elsevier.com/locate/molliq

Deep eutectic solvents interaction with asphaltenes: A combined experimental and molecular dynamics study

Akshatha Hebbar [a], Devangshi Debraj [a], Sriprasad Acharya [a], Sampath Kumar Puttapati [b], Anoop Kishore Vatti [a,*], Poulumi Dey [c,*]

[a] Department of Chemical Engineering, Manipal Institute of Technology (MIT), Manipal Academy of Higher Education (MAHE), Manipal, Karnataka, 576104, India
[b] Department of Chemical Engineering, National Institute of Technology, Warangal, Telangana, 506004, India
[c] Department of Materials Science and Engineering, Faculty of Mechanical, Maritime and Materials Engineering (3mE), Delft University of Technology, 2628 CD Delft, the Netherlands

ARTICLE INFO

Keywords:
DES
Asphaltene
Optical microscopy
FTIR
Molecular dynamics simulations

ABSTRACT

Deep eutectic solvents (DESs) are industrially promising solvents and posses numerous applications in wide areas such as metal processing, synthesis media, synthesis of nanoparticles, gas sequestration and many more. In this work, we synthesized and investigated the performance of three deep eutectic solvents (DESs) i.e., reline, glyceline and ethaline in the separation of pure asphaltene from organic solvents, i.e., toluene and n-heptane using experimental techniques and classical molecular dynamics (MD) simulations. The DESs are prepared and characterized by Fourier transform infrared (FTIR) spectroscopy and density meter analysis. The separation and aggregation of asphaltene from the organic solvent phase into the DES phase at various DES concentrations are visually observed using optical microscopy. MD simulations are used to probe the end-to-end distance and diffusion coefficient of the asphaltene molecules in DESs-organic solvent mixtures. Further, the trajectory density contours of asphaltene in three DESs-toluene/n-heptane systems are calculated to analyze asphaltene aggregation in the presence of the DESs. Our experimental-simulations synergistic study shows the superior performance of glyceline DES in toluene and reline DES in n-heptane for efficient separation of the asphaltene.

1. Introduction

Asphaltenes are the heaviest components of crude oil and constitute the highest fraction of heavy crude oil. They are identified as an ether-insoluble fraction of asphalt in the distillation residue of petroleum [1–3] and are one of the four classes of heavy crude oil, often referred to as SARA: saturates, aromatics, resins, and asphaltenes. Asphaltenes are non-biodegradable, have high viscosity [4,5], and tend to precipitate and stabilize oil-water emulsions during heavy oil recovery. Hence, they can cause serious problems in petroleum refinery operations, ranging from coke and sludge formation to catalyst deactivation and pipe blocking [6,1,7,8,5,9]. With the world relying on increasing heavy crude oil production with enhanced oil recovery strategies, studying asphaltenes and methods of their removal is imperative to petroleum productivity and optimum utilization of depleting oil reserves [10].

Experimental evidences and theoretical simulations have proposed mechanisms explaining the structure and aggregation behaviour of asphaltenes in organic solvents [11,12]. The well-known Yen-Mullins model suggests that asphaltene molecules form nano-aggregates and then macro–aggregates. This occurs due to the π-π interactions between the polyaromatic cores [13–15]. Asphaltenes are soluble in aromatic solvents such as toluene, pyridine and benzene but exhibit limited solubility in straight-chain alkanes such as n-hexane, n-heptane etc. [16,17]. Hence, such solvents could be employed for asphaltene recovery. Another strategy is to use amphiphilic surfactants with a similar structure as resins to aid in stabilisation of asphaltene in crude oil and inhibition of asphaltene precipitation [6,18,15]. Upgradation of asphaltenes to obtain high-value products heavily depends on the energy required to chemically break asphaltenes into smaller molecules and could be energy and cost intensive if the average molecular weight of asphaltenes dispersed in the oil is very high [6]. Another route to separate asphaltenes from oil could be taken in such cases. Non-polar solvents have conventionally been used to precipitate asphaltenes in order to separate them from vacuum distillation residue and obtain de-asphalted oil [19]. The selection of the method depends on the average molecular weights of the asphaltene in the oil sample and the overall ease of the process

* Corresponding authors.
E-mail addresses: anoop.vatti@manipal.edu (A.K. Vatti), P.Dey@tudelft.nl (P. Dey).

https://doi.org/10.1016/j.molliq.2023.122627
Received 26 May 2023; Received in revised form 6 July 2023; Accepted 18 July 2023
Available online 24 July 2023

of separation, along with other physical properties of the materials involved [6].

However, the conventional chemicals mentioned above often cause environmental, health, and safety concerns, including process safety hazards, toxicological problems, and waste management issues [20]. As these concerns pile up in the form of increased demand for solvents, there is a need to turn to green chemistry to provide feasible alternatives to hazardous chemicals. Studies have reported the relevance of plant-based terpenes and limonene as potential asphaltene inhibitors [21,22]. Other potential candidates in this field are ionic liquids (ILs) due to their low vapour pressure, wide ranges of solubility, and high boiling points that make them recyclable [23,24]. Recent research has extensively focused on the influence of various ILs on the behaviour of asphaltenes [25,15,26,27] through a combination of experiments and molecular dynamics (MD) simulations [28–31].

Celia-Silva et al. [32] studied the behaviour of asphaltenes in the presence and absence of 1-alkyl-3-methylimidazolium ILs using classical MD simulations and density functional theory (DFT) calculations. The DFT calculations showed that asphaltene aggregation was more pronounced in the presence of ILs with longer alkyl chains and halide ions with a lower radius. Dong et al. [24] employed IL polymers functionalised with alkyl chains, cationic imidazole groups and $TFSI^-$ (bis(trifluoromethane) sulfonimide)/DEHP ([phosphoric acid bis(2-Ethylhexyl)]) anions to inhibit the aggregation of asphaltenes, hence improving the viscosity of oil. The interactions within asphaltene agglomerations were replaced by strong hydrogen bonds formed between asphaltene and the polymers, reducing the size of the aggregates by 80%. Despite the successes of ILs, they pose numerous challenges ranging from high costs, limited potential for scale-up, toxic precursors, and complicated and time-consuming synthesis procedures [33].

Deep eutectic solvents (DESs), a neoteric class of organic solvents, have become an increasingly popular alternative to the ILs [34]. They have similar physicochemical properties but do not generate as much waste as ILs, making them far more economical [35]. Methods of preparation of DESs involve less tedious chemical transformations and reagents compared to ILs [36]. Usually, they involve heating, grinding, freeze-drying, solvent evaporation, or recrystallization [37,38]. Often considered a sub-category of ILs, DESs are made of a complex between a hydrogen bond-acceptor (HBA) salt (often quaternary ammonium salts) and a hydrogen-bond donor (HBD). At a particular molar composition of constituents, the resulting mixture is characterised by a low glass transition temperature thereby giving it the property of being a “eutectic mixture” [35]. DESs can be classified as Type I, II, III, IV or V depending on the chemical nature of the constituents used as HBAs and HBDs. Type III DESs can be prepared from less toxic and readily available precursors such as choline chloride or choline acetate as HBAs and urea, glycerol, and ethylene glycol as HBDs. This class of DESs has been widely used in liquid-liquid extraction and separation studies [39–41]. COSMO-SAC (COnductor-like Screening MOdel - Segment Activity Coefficient) was used to ascertain the interactions between methanol and HBA and HBD molecules [42]. The studies reported a higher hydrogen bond accepting capacity for ChCl compared to other HBAs such as mono-ethanolamine chloride, tetrabutylammonium bromide and betaine, thus ensuring higher efficiency of azeotropic separation of methanol - dimethyl carbonate mixtures. Similar analyses on glyceline and ethaline reported σ-distribution curves indicated a higher hydrogen bonding capacity of ChCl with water, facilitating the separation of water–isopropanol azeotropes [43]. Hence, ChCl, being widely studied and also versatile in hydrogen bonding interactions with various types of molecules, is a good choice for an HBA.

Even though DESs are a recent finding, few studies showed their applications to chemical enhanced oil recovery [44,45], and asphaltene treatment, implementing two approaches for efficient oil recovery (i.e., inhibition of asphaltene precipitation [17,18,15,46,47] and separation of asphaltenes from the oil fractions before entering the refining process [48–50]). The selection of either method depends on the average molecular weights of the asphaltene in the oil sample and the overall ease of separation of the process, among other physical properties of the materials involved.

Classical MD simulations have also been extended to study asphaltene aggregation and asphaltene-solvent interactions. Headen et al. [51] simulated island, archipelago and continental asphaltene structures in toluene and n-heptane, and reported the radius of gyration, density, average cluster size and relative shape anisotropy of asphaltenes in the presence and absence of resins. Clusters with an average aggregate number of 3.6-5.6 molecules were observed, with a continuous distribution of cluster sizes, which were congruent with experimental observations. A combination of experimental and MD simulation studies characterized the nature of rods-like asphaltene aggregates formation in toluene – n-hexane mixtures [3]. Analysis of optical microscopy images quantified the increase in aggregates with further addition of hexane. Constant end-to-end distance of asphaltene aggregates indicated the presence of stable aggregates. Diffusion coefficient and trajectory density contours showed the formation of numerous denser aggregates, leading to a decrease in the diffusion coefficient of asphaltene molecules at higher hexane concentrations.

Ghamartale et al. [52] conducted MD simulations on asphaltene – n-heptane systems in the presence and absence of octyl phenol and two ionic liquids: 1-butyl-3-methylimidazolium chloride ([BMIM][Cl]) and 1-butyl-3-methylimidazolium bromide ([BMIM][Br]). Structural attributes of asphaltenes, such as the number of aromatic rings, type and location of heteroatoms and alkyl chain length, were considered to determine the extent of aggregation. Radial Distribution Functions (RDF), asphericity index and angle distribution analyses were employed to differentiate between various orientations of asphaltene clusters such as face-to-face, offset stacked or T-shaped.

Recently, experimental [53,54] and MD [55,56] simulations have been extensively used to study the nature and properties of DESs. Shah et al. [57] reported the molecular interactions of reline and aqueous reline using experiments and molecular simulations. The simulations helped in explaining the lower melting point of reline based on the urea–anion interaction. The effects of water on DESs were classified into different regimes. Water at lower mole fractions enhanced urea-urea interactions, while fractions greater than 25% hydrated the components of reline individually, which was reflected in the investigated transport properties. Celebi et al. [56] investigated the thermodynamic and transport properties of DESs at different water concentrations. The authors tested varying densities and viscosities of reline and ethaline as the water content was increased at different temperatures. With an increase in water content, there was a decrease in density and viscosity of the DESs. Further, reline showed a higher viscosity than ethaline due to the stronger hydrogen bonds with urea.

Pulati et al. [48] demonstrated the use of reline to separate bitumen from Alberta and Utah oil sands at room temperature, using naphtha as a diluent. Laboratory separation tests indicated the influence of a significant density difference and immiscibility of reline in the oil, resulting in a sharp phase separation between the diluted bitumen and the oil sand. Centrifugation and the incorporation of water (up to 25% by weight) in reline showed positive effects on separation, creating three clear phases: bitumen, reline and oil, achieving a yield of 90% after a counter-current extraction of Alberta oil. Kashefi et al. [17] probed the performance of choline chloride/phenyl acetic acid DES (1:1 molar ratio) on an oil sample from Iran (2.1% initial asphaltene composition by weight) and compared with lauric acid, octyl phenol, dodecyl amine, and a commercially available inhibitor. The onset of precipitation was tested by titrating the samples with n-heptane, followed by a visual inspection using an optical microscope. The octyl phenol and DES performed best in delaying the onset of asphaltene precipitation. The presence of acidic and polar phenol, carboxylic acid and amine functionalities in the different inhibitors aided in stabilizing asphaltene. Despite a lower percentage reduction in particle size (41%) using DES

compared to octyl phenol (55%), the lower toxicity and environmental impact of the DES could establish it as a likely candidate.

Jahangiri et al. [18] investigated the choline chloride/ethylene glycol DES (1:1 molar ratio) as an asphaltene precipitation inhibitor. The samples were quantified by Ultraviolet (UV)-visible spectrometry, dynamic light scattering and visually confirmed with the help of an optical microscope, using various ratios of toluene/n-heptane. Results showed a shift in the minimum absorption intensity from an n-heptane/toluene ratio of 1 to 1.2 after adding DES. Further, it was observed that more precipitant is needed for precipitation to occur when DES is present in the mixture. Sanati et al. [15] conducted an experimental study using three hydrophobic DESs, prepared from methyltrioctylammonium chloride (Aliquat 336) as the common HBA and propanol, 1,3-propanediol and glycerol as the HBDs, respectively. Their performance was compared with an IL trihexyl-tetradecyl-phosphonium bis(2,4,4-trimethylpentyl)phosphinate (TTPBP) and a commercially available inhibitor. UV-Visible spectrometry was employed to analyse the onset and kinetics of asphaltene precipitation, adding 1% (by weight) of DES and varying concentrations of n-heptane to the asphaltene/toluene system. The DES with glycerol as its HBD, and TTPBP showed superior performance, validated by a significant delay in precipitation onset. A higher number of hydroxyl functionalities in glycerol facilitated stronger hydrogen bonding interactions of the DES with the asphaltene, overpowering the cohesive forces between the asphaltene molecules. This also resulted in partial disruptions in the asphaltene structure, which explained the drastic dip in thermal stability and lower aromaticity index of the asphaltenes recovered from these samples when subjected to Fourier Transform Infrared Spectroscopy (FTIR), Thermogravimetric analysis (TGA) and elemental analysis.

Hu et al. [50] investigated the effects of three ILs and three DESs (reline, ethaline and maline) as solvents to extract asphaltene from oily sludge. The authors found that increasing the water content in the DESs enhanced their oil extraction efficiency. Adding up to 40% water in the DES increased conductivity and reduced viscosity, which in turn helped enhance oil recovery. However, once the water content level exceeded 60%, the amount of oil extracted tended to decrease. Ethaline performed the best, with each DES showing an oil recovery rate of 40% of the liquid mass. Machine learning algorithms were employed to quantify the relationship between the physical properties of the solvents (viscosity, conductivity, surface tension and pH) and the extraction efficiency. The ridge regression algorithm yielded results closest to the experimental values. Once the data was normalised, it was found that the most critical factor affecting oil recovery efficiency was conductivity, followed by pH, surface tension, and viscosity.

This overview of recent investigations highlights the importance of utilizing greener solvents like DESs in the recovery of oil over conventional organic solvents and expensive ILs. However, most of the existing research focusses on methods of inhibition of asphaltene precipitation. Hydrophilic ChCl-based DESs have also been reported as a good choice for separation [48,50] and favourable asphaltene-DES interactions [17,18]. The immiscibility of such DESs in organic media increases the effectiveness of solvent recovery, making DESs potential solvents for asphaltene separation. However, there are very few experimental and in-silico studies in existing literature specifically dealing with asphaltene separation using DESs and a combined experimental and MD investigations is required. To the best of our knowledge, existing literature lacks such a comprehensive study. Our work aims to combine insights from MD simulations and experiments to synthesize, characterize, assess, and compare the performance of three DESs, i.e., reline, glyceline, and ethaline. We thoroughly investigated the interactions of our chosen DESs with asphaltene in the presence of toluene and n-heptane solvents and the subsequent separation of asphaltenes into the DES phase, using MD simulations, densitometer analysis, FTIR spectroscopy, and optical microscopy. Furthermore, we report the end-to-end distance, diffusion coefficients, and trajectory density contours to quantify the extent of asphaltene aggregation in DESs.

Table 1
Molar ratios of the synthesized DESs, notations used, and experimental conditions maintained during synthesis are summarized in the table.

Notation	S1	S2	S3
DES	Reline	Glyceline	Ethaline
Mixture	S1 (ChCl:Urea)	S2 (ChCl:Glycerol)	S3 (ChCl:EG)
Molar ratio	1:2	1:2	1:2
Time of preparation (min)	120	40	30
Pressure maintained (mbar)	45	3	30
Temperature of water bath °C	50	40	50
Rpm of rotary evaporator	14	22	36

2. Experimental details

95% pure asphaltene (Violanthrone-79) ($C_{50}H_{48}O_4$) was procured from BLD Pharmatech, Limited. Toluene (99%) and n-heptane (99%) were used as organic solvents and sourced from Loba Chemie Ltd. Raw materials for the preparation of DESs, namely, choline chloride (ChCl) (98%), urea (99%), glycerol (98%), and ethylene glycol (EG) (99%) were obtained from Loba Chemie Ltd. Choline chloride HBA was kept in a vacuum-oven overnight to remove any free moisture. The required amounts of choline chloride and the respective HBDs were measured (HBA: HBD ratio of 1:2) and added to a round-bottomed flask. The components were then mixed in the rotary vacuum evaporator and heated in a water bath until a homogeneous transparent liquid was formed [58]. DES molar ratios, notations used, and experimental conditions maintained during preparation are specified in Table 1. Reline, glyceline, and ethaline are labelled as S1, S2, and S3, respectively. The DESs in asphaltene-toluene/n-heptane samples were probed using two primary methods: filter paper [59] and microscopic methods [60,61,3,31]. The methodology adopted for the sample preparation and the filter paper method is described in detail in our recent work [3]. The samples were prepared and transferred in a petri dish. During optical imaging, petri dishes were closed with the lid to avoid the evaporation of the organic solvents. The Olympus IX73 inverted microscope was used to capture the images. FT/IR-6300 (Jasco) was used for the FTIR, and the samples were scanned with a scanning resolution of 0.07 cm^{-1} and in the wavenumber range of 500 to 4000 cm^{-1}. The densities of pure DES samples were determined in a temperature range of 288.15 K to 333.15 K at intervals of 10 K at atmospheric pressure, using a DMA1001 digital density meter from Anton Paar. The standard deviations associated with the repeatability and reproducibility of measurements are 0.00005 and 0.00007 g/cm^3, respectively.

The variations in densities of pure reline, glyceline, and ethaline with temperature changes are analysed experimentally and compared with values reported in earlier experimental works for reline [62,54], glyceline [63,53,64,54,65,66] and ethaline [67,54,65]. Densities of 1.196, 1.189, and 1.116 g/cc at 298.15 K were observed for reline, glyceline and ethaline, respectively. This difference in densities of these three DESs has been attributed to variations in the type and extent of hydrogen bonding between the HBA and HBD, which has been presented in detail by Hansen et al. [68]. As evident from Fig. 1, the densities of all three DESs decrease with an increase in temperature, owing to the effects of thermal expansion [67]. Yadav et al. [63,53] concluded that the density-temperature relationships of each DES follow a linear relationship up to temperatures of 323.15 K, which agrees with our results. While the density data for reline agrees with the data reported by Haghbakhsh et al. [62], deviations were observed with respect to the data reported by Crespo et al. [54] (average deviation of 0.002 g/cc). We report minimal density deviations for ethaline compared to existing literature (average deviation of <0.0009 g/cc). Lower density values with temperature (average deviation of 0.001 g/cc) were observed for glyceline compared to other experimental observations [65,66], while the linearity and extent of change remained the same.

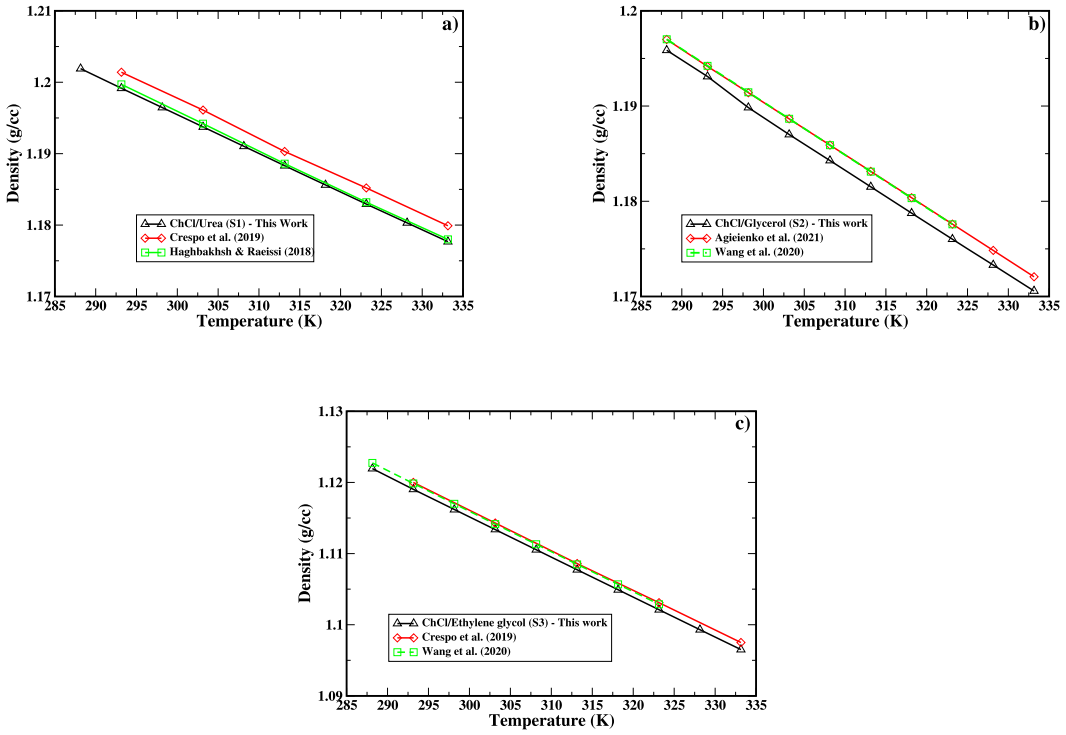

Fig. 1. Density variation with temperature (a) Reline (b) Glyceline (c) Ethaline. Our results are compared with those in the literature.

3. Computational details

The molecular mass of asphaltene compounds ranges from 500 to 1000 g/mol [69], and the average molecular mass is approximately 750 g/mol [11]. Violanthrone-79 has a molecular weight of 712.9 g/mol, which is close to the representative value of 750 g/mol. Structurally, this molecule consists of a polyaromatic core, with two aliphatic side chains and oxygen atoms making up two aromatic ketone and aliphatic ester functionalities. Studies on the quantitative molecular representations (QMR) of asphaltenes reported that such peri-condensed asphaltene structures could better represent experimental data in comparison to higher molecular weight asphaltenes [70]. Moreover, the structure of this compound also approximates the final optimised structures having an island-type polyaromatic core flanked with alkyl side chains, which is also observed in the structure of asphaltene by Headen et al. [13,21]. Thus, we chose Violanthrone-79 as model asphaltenes for our simulations. In addition to Violanthrone-79, toluene, n-heptane, S1, S2, and S3 explicit DES molecules are considered in the MD simulation. The various combinations of solvents and DESs used in the study are listed in Table 2. Our simulation boxes contain approximately 5 wt% of the DESs. Optimized Parameters for Liquid Simulations (OPLS4) [71] force fields are used to describe the bonded and Lennard-Jones interactions in the model. Desmond [72] MD code is used within the Schrödinger simulation software [73], using a time step of 2 fs to integrate the equations of motion. A 9 Å cut-off is considered for non-bonded interactions. Martyna-Tobias-Klein barostat with isotropic coupling having a relaxation time of 2 ps and Nose-Hoover thermostat with a relaxation time of 1 ps are used. The NPT equilibration run and an NVT production run of 20 ns and 80 ns, respectively, are performed. The temperature of 300 K is considered for NVT run and pressure of 1 atm and 300 K for NPT run.

The MD snaphots of the asphaltene in toluene, asphaltene in toluene and reline, asphaltene in toluene and glyceline and asphaltene in toluene and ethaline are shown in the Fig. 2 (a), (b), (c) and (d), respectively. Similarly, the MD snaphots of the asphaltene in n-heptane, asphaltene in n-heptane and reline, asphaltene in n-heptane and glyceline and asphaltene in n-heptane and ethaline are shown in Fig. 3 (a), (b), (c) and (d), respectively. The snapshots clearly show the aggregates of the asphaltene molecules as depicted by the green colour in the presence of the DESs where the aggregates can be seen more clearly in n-heptane than in the toluene solvent.

4. Results and discussion

4.1. Optical microscopy

We used optical microscopy to visualize asphaltene aggregation in DESs, an analogous approach as used in our previous studies [3,31]. Fig. 4 (a) shows the optical image of asphaltene in toluene for which no aggregations were observed as the asphaltene molecules remain stable and dissolve in toluene due to steric repulsions between their alkyl chains [74]. Figs. 4 (b), (c), and (d) show the optical images of 0.1 mL of S1, S2 and S3 added to the asphaltene-toluene solution, respectively. All three figures (i.e. (b) to (d)) show a distinct phase separation between toluene and DESs. The toluene, DESs and their interface are depicted in blue, white and light blue colours, respectively. No distinct aggregates were observed in these three samples. We then increased the concentration of the DESs to 0.2 mL. Figs. 5 (b), (c), and (d) show the optical images of 0.2 mL of S1, S2 and S3 added to the asphaltene-toluene solution, respectively. In this particular case, distinct needle-like, branched aggregates with some degree of stacking were observed as can be seen in Figs. 5 (b) and (d). The aggregates were initially observed to form at the toluene-DES interface which eventually moved into the DES phase within a shorter time span. In contrast, aggregates in S2, as shown in Fig. 5 (c), have a different morphology, being thicker and rod-like, forming a greater network of branching and stacking after penetrating the S2 phase. Judging by the extent of aggregation, it can be stated that S2 performs better than S1 and S3 in the presence of toluene.

Fig. 6 (a) shows the optical image of asphaltene in n-heptane. A polarity difference between the two species leads to weak molecular interactions, causing asphaltene to destabilise and flocculate as thick, rod-like, and unbranched aggregates. Figs. 6 (b), (c), and (d) show the optical images of 0.1 mL of S1, S2 and S3 added to asphaltene-n-heptane, respectively. We observed an instantaneous pull of the asphal-

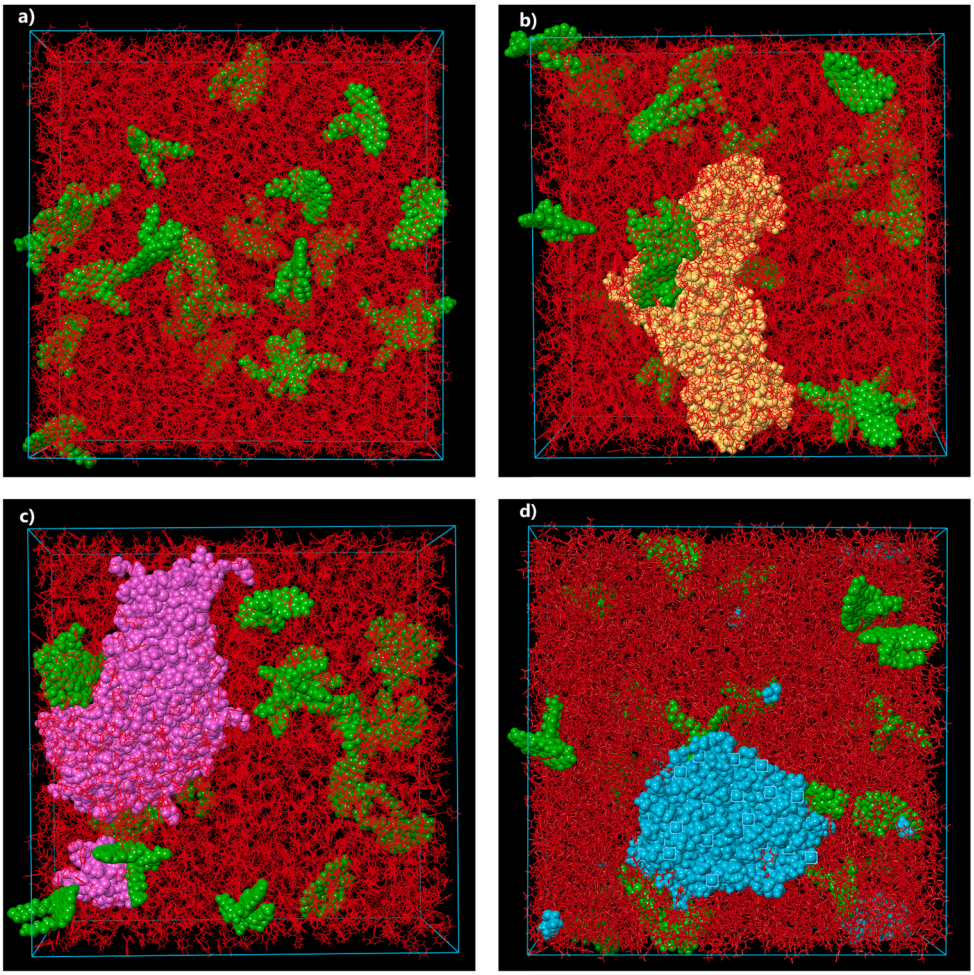

Fig. 2. Snapshots of the MD NVT run showing asphaltene in 4 different systems (a) asphaltene in toluene (b) asphaltene in toluene and reline (c) asphaltene in toluene and glyceline and (d) asphaltene in toluene and ethaline. The colour coding is as follows: asphaltene is green, toluene is red, reline is yellow, glyceline is pink and ethaline is sky blue.

Table 2
The number of asphaltene, toluene, n-heptane and DES molecules, along with the simulation box sizes for considered mixtures are summarized in the table.

Mixture	Asphaltene molecules	Toluene molecules	n-heptane molecules	DES molecules	Simulation Box Size (Å^3)
Asp+Toluene	24	4976	–	–	83.27×104.25×102.95
Asp+Reline (S1)+Toluene	24	4976	–	(ChCl:Urea) 100:200	97.96×98.39×96.40
Asp+Glyceline (S2)+Toluene	24	4976	–	(ChCl:Glycerol) 100:200	97.39×98.18×98.30
Asp+Ethaline (S3)+Toluene	24	4976	–	(ChCl:EG) 100:200	101.16×88.70×104.16
Asp+n-heptane	24	–	4976	–	107.87×107.81×107.73
Asp+Reline (S1)+n-heptane	24	–	4976	(ChCl:Urea) 100:200	108.82×109.01×109.11
Asp+Glyceline (S2)+n-heptane	24	–	4976	(ChCl:Glycerol) 100:200	108.95×109.20×109.60
Asp+Ethaline (S3)+n-heptane	24	–	4976	(ChCl:EG) 100:200	110.12×108.53×108.43

tene rods into the DES phase, with S1 having the greatest separation propensity. The S1/n-heptane interface, as shown in Fig. 6 (b), was thoroughly saturated with asphaltene even at a low concentration of 0.1 mL. Lower separation rates were observed for S2 in Fig. 6 (c) and S3 in Fig. 6 (d). The effect of increase in DES concentration on asphaltene separation was investigated by adding 0.2 mL of S1, S2 and S3 into the asphaltene-n-heptane mixture, as shown in Fig. 7. While the asphaltenes were primarily constrained to the DES/n-heptane interface in Fig. 6, further addition of DES prompted a higher density of asphaltene rods further within the DES phase. S2 showed the highest accumulation of asphaltenes within the DES phase, as shown in Fig. 7 (c). The asphaltene aggregates were still more concentrated towards the S1/n-heptane interface, as depicted in Fig. 7 (b), due to reduced mobility caused by an interface already saturated with clusters of asphaltenes. Since S1 enables the highest degree of separation even at low concentrations, it was found to perform better than S2 and S3 in the presence of n-heptane.

The colloidal model explains the self-aggregating behaviour of asphaltenes and their tendency to exist as fully dispersed, micellar structures in a stable environment, such as toluene, forming a sol [75]. While this property is attributed to the presence of fused aromatic rings in asphaltenes leading to π-π stacking, functional groups like ethers and aliphatic side chains also influence the structure of these micelles. Adding DESs to toluene-asphaltene triggers instabilities in the colloid. Compacting of steric layers takes place, leading to a reduction in the repulsive forces exerted by the side chains. This destabilises the asphaltene molecules and decreases solubility parameters, leading to branched

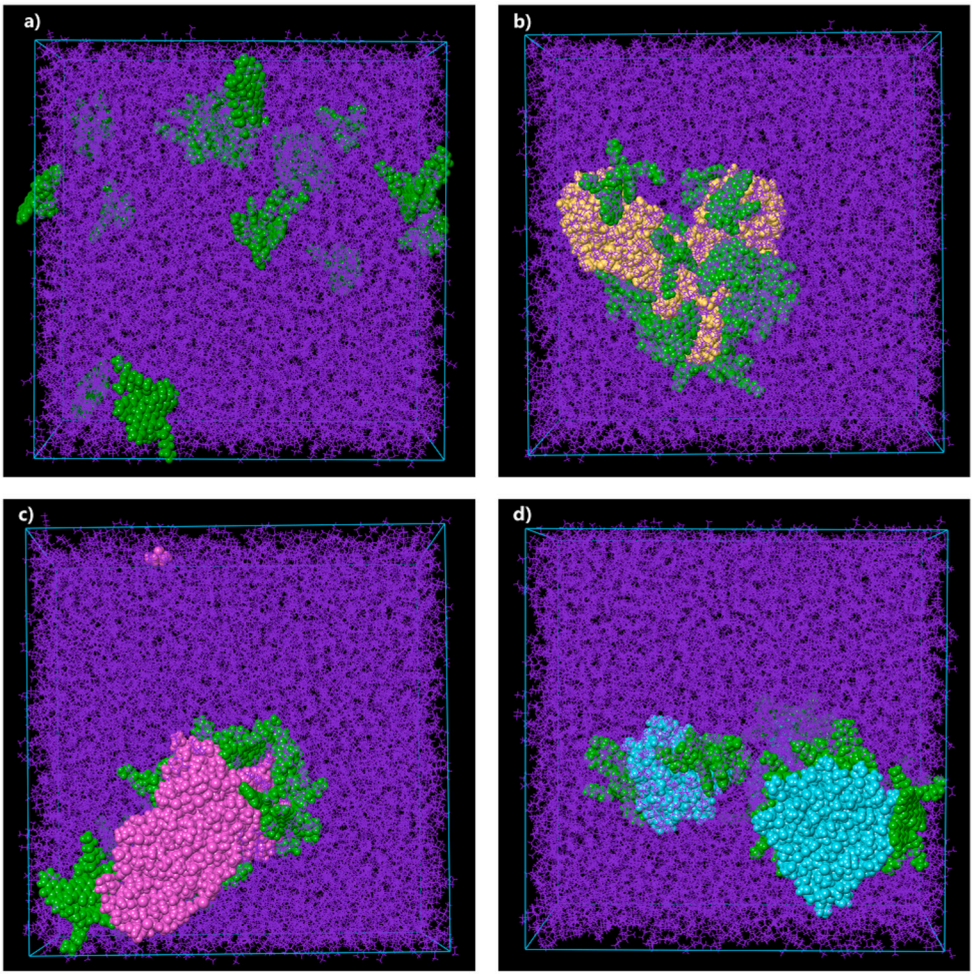

Fig. 3. Snapshots of the MD NVT run showing asphaltene in 4 different systems (a) asphaltene in n-heptane (b) asphaltene in n-heptane and reline (c) asphaltene in n-heptane and glyceline and (d) asphaltene in n-heptane and ethaline. The colour coding is as follows: asphaltene is green, n-heptane is violet, reline is yellow, glyceline is pink and ethaline is sky blue.

aggregates. The solid aggregates continue to grow in volume until the DES phase becomes fully saturated. This phenomenon is termed as 'gelling' [76]. Gel-type asphaltene aggregates are known to confer non-Newtonian characteristics due to highly interconnected structures, π-π, and polar interactions. A close inspection of dilute clusters observed in Fig. 5 (b) leads to a hypothesis that a partial gel-type aggregation of asphaltenes has occurred. S2 tends to trigger higher instabilities in asphaltene, judging by the density of aggregations. Overall, glyceline performed better in the toluene base solution because the extent of aggregation is maximum. Reline performed superior compared to the other DES in n-heptane solvent as the aggregation reaches a saturation point even at lower concentrations of the DES.

4.2. FTIR

The FTIR spectra of pure S1, pure asphaltene, asphaltene-toluene solution, and asphaltene-toluene-0.2 mL S1 are shown in Fig. 8(a) and are represented by black, red, green, and blue lines, respectively. Pure S1 shows a strong pair of peaks at 3266 and 3415 cm^{-1}, which corresponds to primary -NH_2 stretching modes due to the amide functional group in urea. A unique pair of peaks are also obtained at 1682 and 1625 cm^{-1}, representing strong C=O stretching of saturated amides coupled with N-H deformations. The peak at 1465 cm^{-1} signifies C-N stretching vibrations. Signals obtained in the 1000-1300 cm^{-1} and very weak peaks 2917-3000 cm^{-1} range represent C-O, C-C-O stretching vibrations, C-O-H bending vibrations and sp^3 C-H stretching vibrations, all of which are characteristic of choline chloride [77]. This proves that S1 retains the characteristics of both choline chloride and urea. The strong hydrogen bonding interactions between the two molecules are evident due to redshifts in the stretching and bending modes of NH_2 (3266 – 3415 cm^{-1}), C=O stretching peaks (1625,1682 cm^{-1}) and the formation of a broader peak in the 3200-3500 cm^{-1} range.

The FTIR spectra of asphaltene and asphaltene-toluene solutions show prominent peaks in three major regions. Peaks at 3027, 2920 and 2868 cm^{-1} represent aromatic, asymmetric and symmetric C-H stretches, respectively. The range of peaks from 1550 to 1700 cm^{-1} represents C=O stretching, 1570 cm^{-1} represents C=C-C stretching of the polyaromatic rings, and peaks at 1380 and 1480 cm^{-1} represent asymmetric and symmetric CH_3 stretching modes, respectively, as described in detail by our previous study [3]. Two prominent peaks at 692-730 cm^{-1} represent aromatic sp^2 C-H bending vibrations. The FTIR spectra of asphaltene-toluene-0.2 mL S1 show an overlap of all its pure constituents. A sharp decrease in % transmittance and broader peaks are observed at the 692-730, 1380, 1480-1500, and the 2850-3000 cm^{-1} ranges, indicating the presence of asphaltene in the S1 phase separated from toluene. Our earlier studies have also observed and correlated the sharp reduction in % transmittance to an increase in asphaltene aggregates in the sample [3,31].

Changes in % transmission over wavenumber for pure S2, pure asphaltene, asphaltene-toluene solution, and asphaltene-toluene-0.2 mL S2 are shown in Fig. 8 (b) and are represented by black, red, green, and blue lines, respectively. Pure S2 shows peaks in the 851-1110

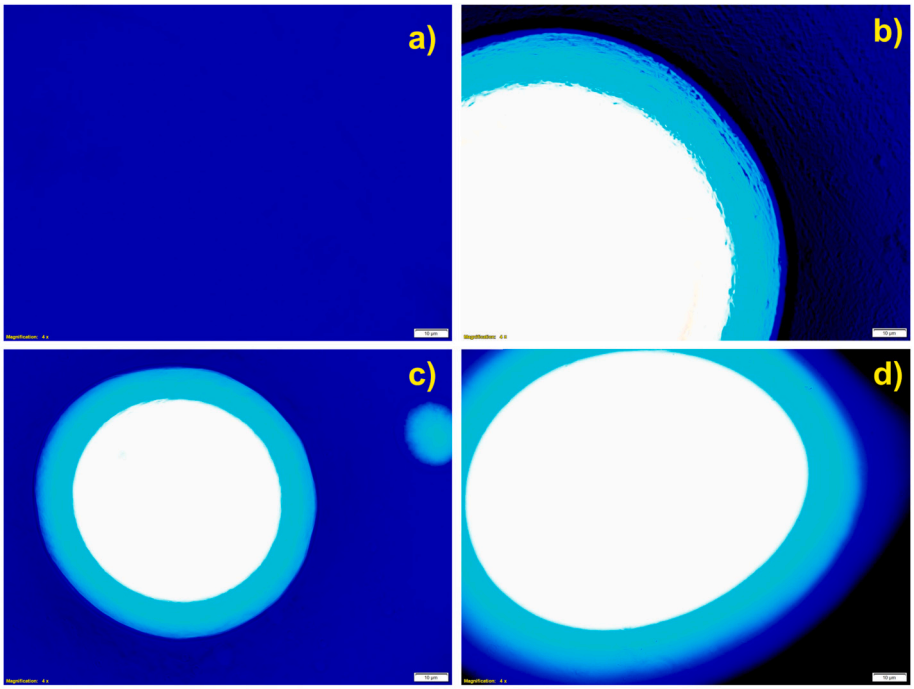

Fig. 4. Optical microscopic images of (a) fully dissolved asphaltene in toluene, (b) asphaltene in toluene along with 0.1 mL reline (S1), (c) asphaltene in toluene along with 0.1 mL glyceline (S2), (d) asphaltene in toluene along with 0.1 mL ethaline (S3). The length scale of each optical image is 10 μm.

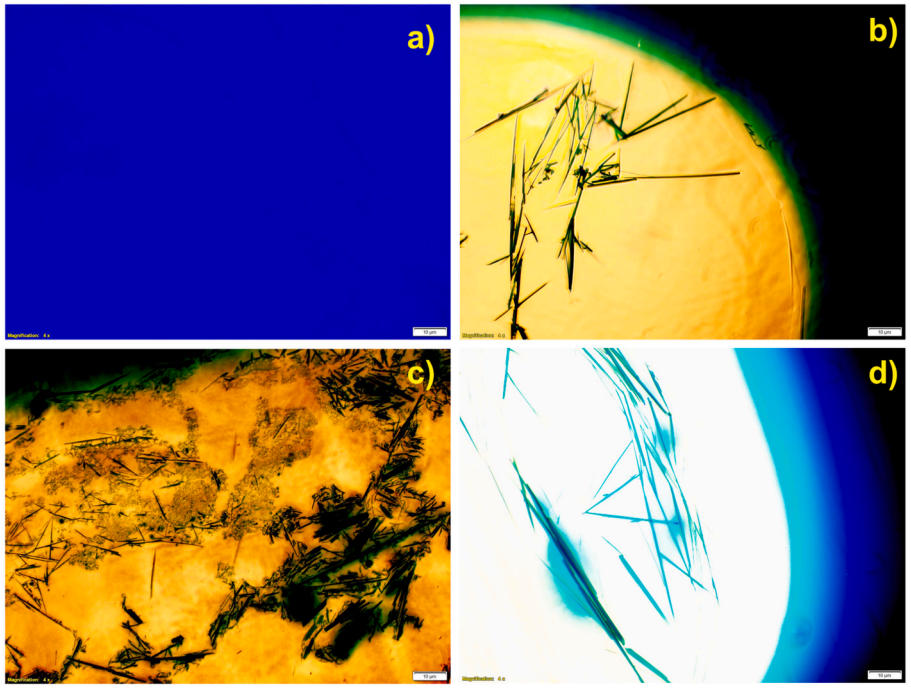

Fig. 5. Optical microscopic images of (a) fully dissolved asphaltene in toluene, (b) asphaltene in toluene along with 0.2 mL reline (S1), (c) asphaltene in toluene along with 0.2 mL glyceline (S2) (d) asphaltene in toluene along with 0.2 mL ethaline (S3). The length scale of each optical image is 10 μm.

cm^{-1} range. Peaks at 851, 924 and 994 cm^{-1} represent C-C vibrations, and peaks at 1038 and 1110 cm^{-1} represent C-O linkage and C-O stretching vibrations, all of which are characteristic of glycerol. Distinct double peaks at 2942 and 2875 cm^{-1} correspond to asymmetric and symmetric C-H stretching vibrations, respectively. Pure S2 has a broad peak in the 3333-3345 cm^{-1} range, representing O-H stretching vibrations. N-H stretching vibrations attributed to choline chloride are also overlapped in this range. Studies in literature have reported similar spectra for pure glyceline and have observed redshifts in the peaks corresponding to O-H and N-H stretching vibrations, indicating the formation of H-bonds between choline chloride and glycerol [77]. Spectra of asphaltene-toluene-0.2 mL S2 are depicted in blue. Although S2 does not show a decrease in % transmittance in the 692-730 cm^{-1} region, intense peaks are observed at 1731 cm^{-1} representing C=O stretching, 1644 cm^{-1} indicating conjugated C=C groups, two peaks at 1284-1320

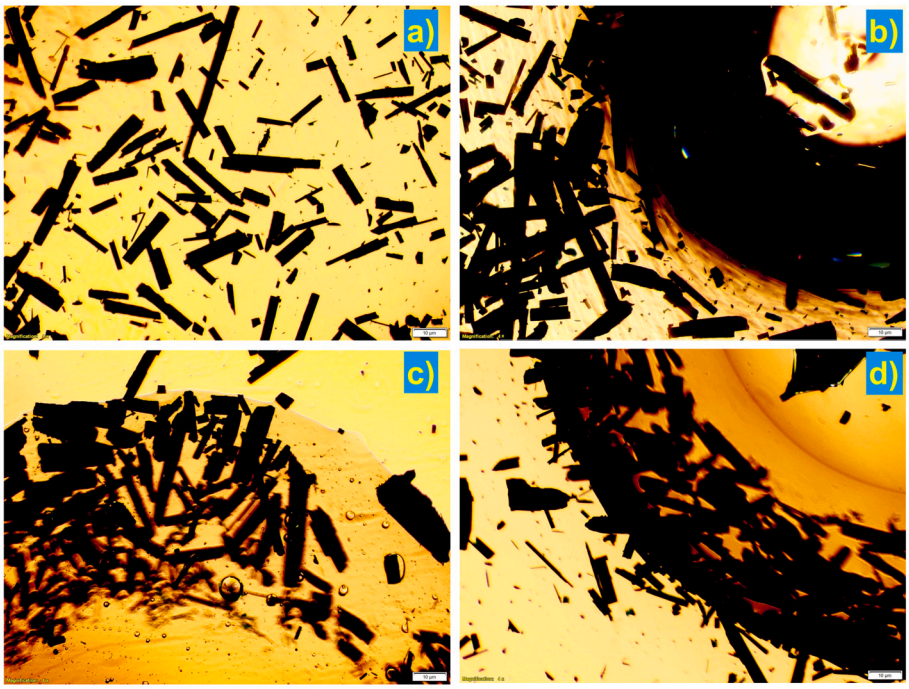

Fig. 6. Optical microscopic images of (a) asphaltene in n-heptane, (b) asphaltene in n-heptane along with 0.1 mL reline (S1), (c) asphaltene in n-heptane along with 0.1 mL glyceline (S2) (d) asphaltene in n-heptane along with 0.1 mL ethaline (S3). The length scale of each optical image is 10 μm.

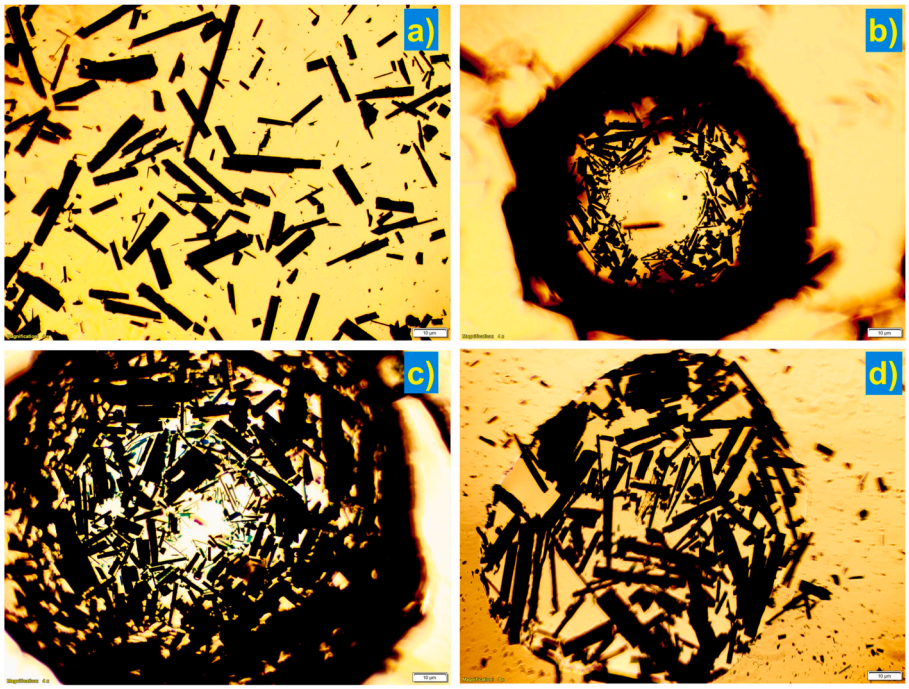

Fig. 7. Optical microscopic images of (a) asphaltene in n-heptane, (b) asphaltene in n-heptane along with 0.2 mL reline (S1), (c) asphaltene in n-heptane along with 0.2 mL glyceline (S2) (d) asphaltene in n-heptane along with 0.2 mL ethaline (S3). The length scale of each optical image is 10 μm.

cm^{-1} indicating C-O stretching vibrations, and a broad peak at 1380 cm^{-1}, indicating CH_3 stretching vibrations.

Fig. 8 (c) represents the FTIR spectra of pure S3, pure asphaltene, asphaltene-toluene solution, and asphaltene-toluene-0.2 mL S3 and are represented by black, red, green, and blue lines, respectively. Owing to a similarity in the structures of glycerol and ethylene glycol, a broad peak in the 3333-3345 cm^{-1} range signifies O-H stretching, and double peaks at 2875-2942 cm^{-1} corresponding to C-H stretching are observed. Peaks at 1500, 1250 and 1000-1100 cm^{-1} represent C-H bending vibrations, alcoholic C-O stretching, and C-O-C and C-O-H bending vibrations, respectively, showing fingerprints of both ethylene glycol and choline chloride [78]. Spectra of asphaltene-toluene-0.2 mL S3 are depicted in blue. An increase in peak intensities at around 1380, 1624, and 1730 cm^{-1} is observed, although the peaks are narrower and less intense than the ones obtained for the corresponding spectra for S1 in Fig. 8 (a) and S2 in Fig. 8 (b). All three spectra of asphaltene-

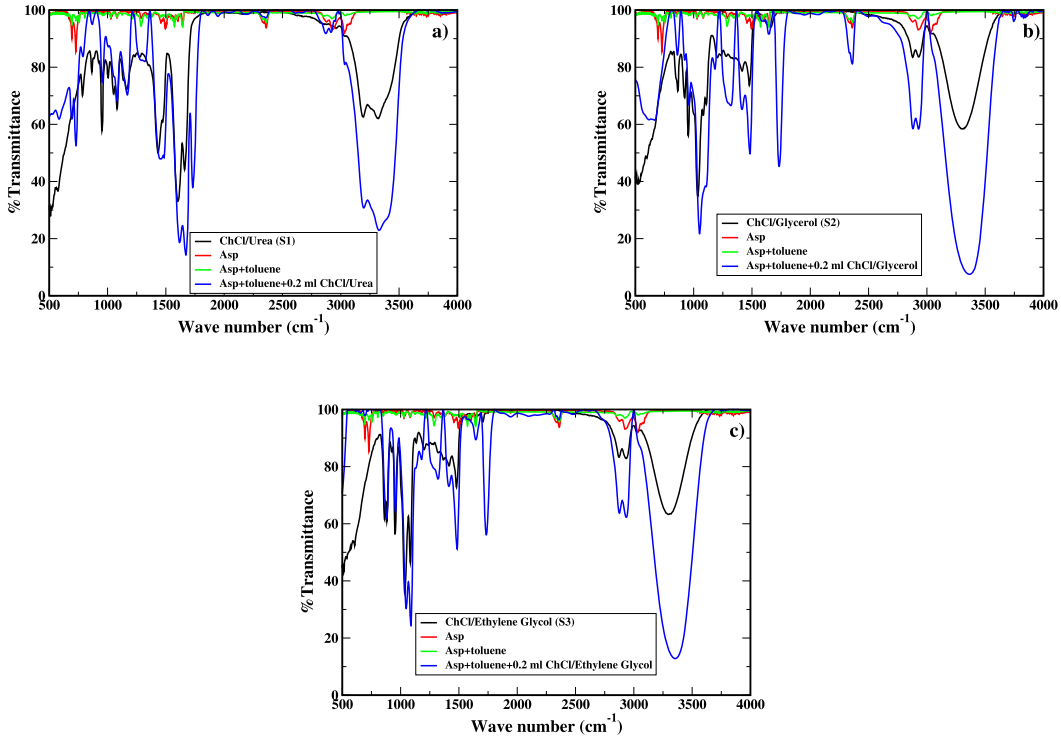

Fig. 8. (a) FTIR spectra of pure reline (S1), pure asphaltene, asphaltene-toluene mixture and asphaltene-toluene-0.2 mL S1 mixture are shown in black, red, green, and blue colour lines, respectively, and (b) FTIR spectra of pure glyceline (S2), pure asphaltene, asphaltene-toluene mixture and asphaltene-toluene-0.2 mL S2 mixture (c) FTIR spectra of pure ethaline (S3), pure asphaltene, asphaltene-toluene mixture and asphaltene-toluene-0.2 mL S3 mixture.

toluene-DES in Fig. 8 exhibit higher peak intensities than their pure constituents, which can be correlated to a higher concentration of asphaltene aggregates in the respective DES phases. Another common observation from the three spectra in Fig. 8 is the presence of a sharp, intense peak at 1732 cm^{-1} corresponding to C=O stretching vibrations in asphaltene-toluene-0.2 mL of all three DESs, which is absent in the spectra of corresponding pure constituents. This could indicate additional interactions due to the aggregation of asphaltene within the DES phase, as corroborated in previous studies for wavenumber ranges of 1550-1700 cm^{-1} [79,3]. The FTIR spectra of pure S1, pure asphaltene, asphaltene-n-heptane mixture, and asphaltene-n-heptane-0.1 mL S1 are shown in Fig. 9 (a) and are represented by black, red, green, and blue lines, respectively. The spectra of n-heptane in the presence of DESs show lower % transmission values compared to toluene due to insoluble rod-like aggregations. A series of weak signals at 2920-2868 cm^{-1}, three broad peaks in the 1500-1580 cm^{-1} range and 3300-3500 cm^{-1}, range are observed. The peak intensities are comparable to those of asphaltene-n-heptane. Fig. 9 (b) depicts the FTIR spectra for pure S2, pure asphaltene, asphaltene-n-heptane mixture and asphaltene-n-heptane-0.1 mL S2. The spectra of asphaltene-n-heptane-0.1 mL S2 mirror the corresponding spectra of asphaltene-n-heptane except at the broad peak corresponding to O-H stretching, with a significant reduction in % transmission. This indicates that the separation of asphaltenes from the n-heptane phase has been captured in the sample. Fig. 9 (c) represents the corresponding spectra for pure S3, pure asphaltene, asphaltene-n-heptane, and asphaltene-n-heptane-0.1 mL S3. There is a direct overlap between the spectra of S3 in asphaltene-n-heptane and pure S3, except for a weak signal at around 1583 cm^{-1}, corresponding to polyaromatic ring stretching.

4.3. End-to-end distance

The end-to-end distance refers to the distance between one end of the alkyl side chain of asphaltene to the other end. It is an important parameter which helps to analyze the size of the aggregates, since during aggregation, the alkyl chains are flexible on longer length scales and stiff on shorter length scales. We have calculated the end-to-end distance of asphaltene molecules in the presence and absence of DESs. In our previous studies, we calculated the end-to-end distance of asphaltene in aqueous media [80], organic solvents [3] and IL [31]. We evaluated the distance using a worm-like chain model [81] taking the semi-flexible side chains into consideration [82]. The molecule-averaged end-to-end distance over the entire MD production run trajectory is calculated using the following equation [82]:

$$\left\langle R_E^2 \right\rangle = 2 l_P L_0 \left[1 - \left(l_P / L_0\right)\left(1 - exp\left(-L_0 / l_P\right)\right)\right] \quad (1)$$

Where $\left\langle R_E^2 \right\rangle$, l_P and L_0 denote the mean squared end-to-end distance, persistence length and extended chain length, respectively.

The variation in the end-to-end distance as a function of simulation time for asphaltene-toluene in S1 is shown in Fig. 10 (a). Fig. 10 (b) represents the frequency distribution of end-to-end distances for asphaltene-toluene in S1. Table 3 summarizes the end-to-end distance, persistence length, and extended chain length, as well as the standard deviations of time series and molecular distribution for all eight combinations considered in the study. The end-to-end distance of asphaltene molecules in pure n-heptane (11.48 Å) is slightly lower than that in pure toluene (11.87 Å), demonstrating the insolubility of asphaltene in n-heptane, leading to a strong tendency of aggregation. Lower end-to-end distances also indicate closer proximity of alkyl side chains, signifying greater stability of aggregates.

When S1 or S2 is added to the asphaltene-toluene mixture, a slight decrease in the end-to-end distance compared to the asphaltene-toluene mixture, i.e., 11.86 Å and 11.71 Å, respectively, is observed. In contrast, the end-to-end distance increased to 12.03 Å with the addition of S3 to the asphaltene-toluene mixture. A slight decrease in the end-to-end distances is observed when DESs are added to the asphaltene-n-heptane mixture, indicating a higher separation of asphaltene into the DES phase. The lowest values were observed for the S3-asphaltene-n-heptane combination (10.95 Å). The values remained

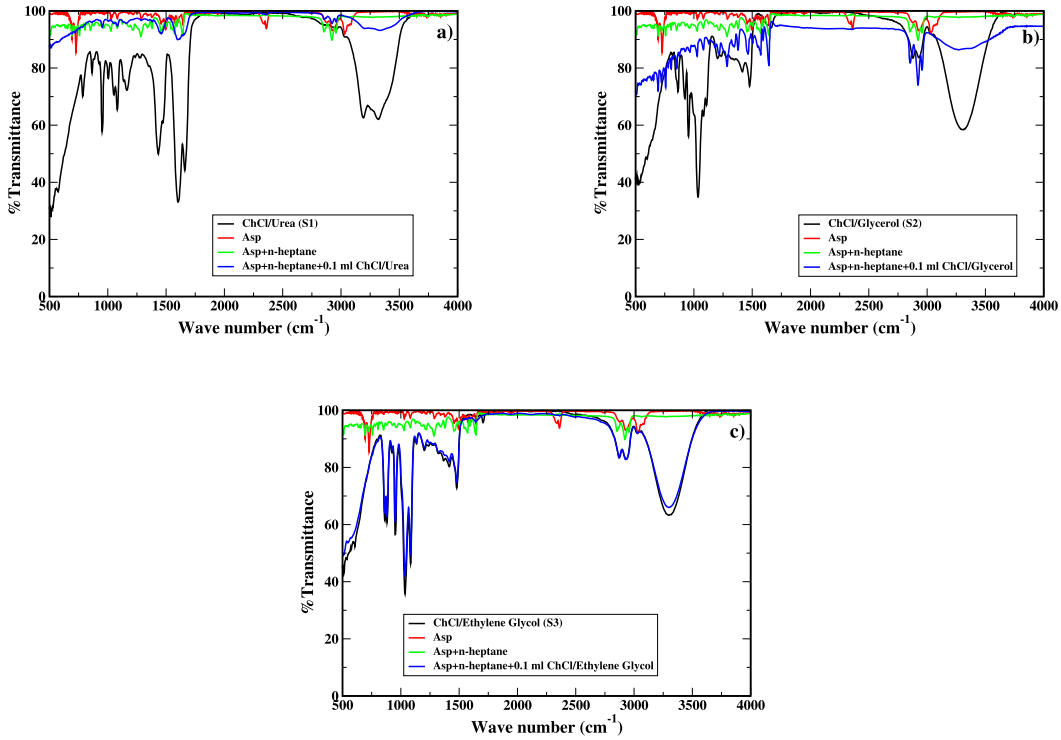

Fig. 9. (a) FTIR spectra of pure reline (S1), pure asphaltene, asphaltene-n-heptane mixture and asphaltene-n-heptane-0.1 mL S1 mixture are shown in black, red, green and blue colour lines, respectively. (b) FTIR spectra of pure glyceline (S2), pure asphaltene, asphaltene-n-heptane mixture and asphaltene-n-heptane-0.1 mL S2 mixture. (c) FTIR spectra of pure ethaline (S3), pure asphaltene, asphaltene-n-heptane mixture and asphaltene-n-heptane-0.1 mL S3 mixture.

Table 3
The calculated end-to-end distance of asphaltene molecules, extended chain length, persistence length, time series standard deviation (σ) related to the end-to-end distance and molecular distribution standard deviation values are shown for different asphaltene-solvent-DES mixtures over 80 ns of production run.

Mixture	End-to-end distance (Å)	Persistence length (Å)	Extended chain length (Å)	Time Series (σ (Å))	Molecular Distribution Standard Deviation (Å)
Asp+Toluene	11.87	3.81	24.53	0.83	4.16
Asp+Reline (S1)+Toluene	11.86	3.80	24.54	0.83	4.14
Asp+Glyceline (S2)+Toluene	11.71	3.70	24.54	0.83	4.12
Asp+Ethaline (S3)+Toluene	12.03	3.92	24.56	0.80	4.14
Asp+n-heptane	11.48	3.54	24.48	0.82	4.02
Asp+Reline (S1)+n-heptane	11.34	3.43	24.54	0.82	4.04
Asp+Glyceline (S2)+n-heptane	11.32	3.41	24.50	0.84	3.96
Asp+Ethaline (S3)+n-heptane	10.95	3.17	24.53	0.88	3.97

uniform in S1-asphaltene-n-heptane and S2-asphaltene-n-heptane (approximately 11.3 Å). Similar results were observed in previous studies using $[BMIM][PF_6]$, $[Et_3NH]^+[CH_3COO]^-$ and $[Et_3NH]^+[H_2PO_4]^-$ ILs, where asphaltenes in IL/n-hexane mixtures showed lower end-to-end distances compared to those in IL/toluene mixtures [31,83]. These variations in end-to-end distances with the solvent/DES environment are attributed to the tendency of the alkyl side chains to adapt to the solvents due to the aggregate formation.

In conclusion, a lower end-to-end distance is observed when asphaltenes are added to n-heptane compared to toluene in the presence of DES due to stable aggregates in n-heptane. An extended chain length of approximately 24.5 Å is observed for all eight mixtures. A molecular distribution standard deviation of 4.06±0.1 indicates that the variations in the end-to-end distances within asphaltene molecules are uniform, irrespective of concentration. The persistence length specifies the length beyond which no correlations are observed, meaning the alkyl side chains are stiffer for distances longer than the persistence length. Interestingly, different persistence lengths are observed for each of the eight mixtures considered in this study, indicating slight differences in the extent of aggregation.

4.4. Diffusion coefficient

The asphaltene molecules diffusion coefficient is calculated using the following equation [84]:

$$D = \frac{1}{6}\lim_{t\to\infty}\frac{d}{dt}\left\langle\left|\vec{x}(t)-\vec{x}(0)\right|^2\right\rangle \quad (2)$$

where mean-square displacement is denoted as $\left\langle\left|\vec{x}(t)-\vec{x}(0)\right|^2\right\rangle$ and angled brackets indicate an ensemble average.

The diffusion coefficient values were obtained based on mean square displacement function versus time. These values were calculated for asphaltene molecules in 8 different solution mixtures as presented in Table 4. We observed that upon adding reline (S1) and glyceline (S2) to toluene the diffusion coefficient value has not drastically reduced, whereas in case of n-heptane where the diffusion coefficient value decreased significantly implying that asphaltene mobility is lowered to a major extent. The lowest value obtained was in the case of asphaltene in n-heptane and reline (S1), i.e. 0.70×10^{-10} m^2/s indicating maximum aggregation occurring in this system, whereas the highest value obtained was in the case of asphaltene in pure n-heptane, i.e., 5.90×10^{-10} m^2/s indicating the highest mobility of asphaltene for this case. The lowest

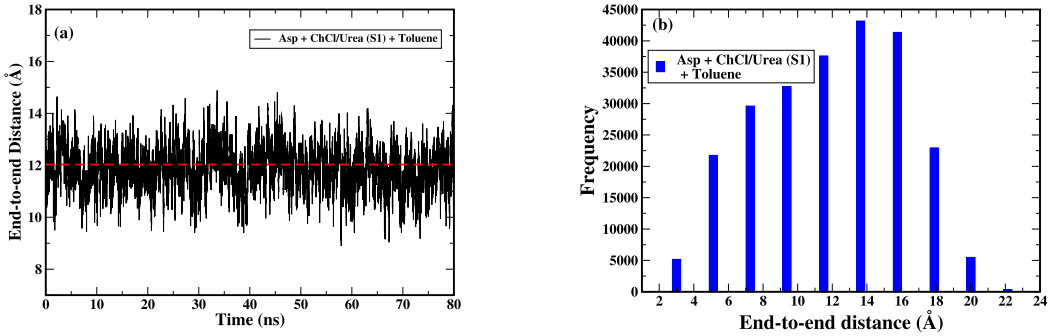

Fig. 10. (a) The calculated end-to-end distance versus time of asphaltene molecules in reline-toluene mixture. (b) frequency versus end-to-end distance of asphaltene molecules in reline-toluene mixture. The averaged end-to-end distance is indicated by a red-dashed line in (a).

Table 4
The calculated diffusion coefficients are shown for eight different asphaltene mixtures.

Mixture	Diffusion Coefficient (m^2/s)
Asp+Toluene	3.59×10^{-10}
Asp+Reline (S1)+Toluene	3.57×10^{-10}
Asp+Glyceline (S2)+Toluene	3.54×10^{-10}
Asp+Ethaline (S3)+Toluene	4.35×10^{-10}
Asp+n-heptane	5.90×10^{-10}
Asp+Reline (S1)+n-heptane	0.70×10^{-10}
Asp+Glyceline (S2)+n-heptane	1.60×10^{-10}
Asp+Ethaline (S3)+n-heptane	1.06×10^{-10}

diffusion coefficient for asphaltene in heptane and reline (S1) suggests that asphaltene aggregates have stronger binding in this case.

4.5. Density contours

The asphaltene trajectory density cross-section is constructed by first dividing the simulation box into cross-sections of a specified thickness, such that the layers are perpendicular to the XY cartesian coordinate axis. The density profile is calculated at a particular location on the axis by following a series of steps. The fraction of the van der Waals volume of each atom overlapping a particular layer is multiplied by its atomic mass. The individual results over all specified atoms are summed up and divided by the volume of the layer. Each layer is then further partitioned into cubes, and the volume fraction of each atom overlapping each cube is calculated. The result is weighted by the atomic mass, added and divided by the volume of the cube, to obtain the density within it.

The asphaltene trajectory density contours for the asphaltene-toluene-DES mixtures are shown in Fig. 11. Fig. 11(a) illustrates the asphaltene trajectory density contour for asphaltene in pure toluene solvent, Fig. 11(b) asphaltene trajectory density contour for asphaltene in toluene-reline DES, Fig. 11(c) shows the asphaltene trajectory density contour for asphaltene in toluene-glyceline DES and Fig. 11(d) shows density contour for asphaltene in toluene-ethaline DES. It is evident from the density contour shown in Fig. 11(a) that the density of asphaltene molecules is spread across the cubic box because of the soluble nature of the asphaltene in toluene, the maximum intensity of the contour, i.e., the red colour is shown all over the box. On the other hand, the aggregation of asphaltene is visible in Figs. 11 (b), (c) and (d) upon addition of the respective DES, i.e., S1, S2 and S3. We observed the formation of slightly delocalized asphaltene aggregates with the addition of the DES in the asphaltene-toluene mixture, as can be seen in Figs. 11 (b), (c) and (d). Based on the trajectory density contours, the glyceline performance is found to be superior as more localized asphaltene aggregates are observed in Fig. 11(c) in comparison to reline and ethaline.

The asphaltene trajectory density contours for asphaltene-n-heptane-DES mixture are shown in Fig. 12. Fig. 12 (a) illustrates the asphaltene trajectory density contour for asphaltene in pure n-heptane solvent, Fig. 12 (b) shows the asphaltene trajectory density contour for asphaltene in n-heptane-reline DES, Fig. 12 (c) shows the asphaltene trajectory density contour for asphaltene in n-heptane-glyceline DES and Fig. 12 (d) shows density contour for asphaltene in n-heptane-ethaline DES. It is evident that because of the formation of the aggregates in n-heptane localized asphaltene aggregates are noticed in Fig. 12 (a). Upon addition of reline, glyceline and ethaline, we noticed that aggregate formation is further pronounced. The performance of glyceline is found to be superior in separating asphaltene from the n-heptane followed by reline and ethaline as evident in the figure which shows localized asphaltene aggregates denoted by the maximum contour density.

5. Conclusion

This work investigated the asphaltene aggregation and separation from two organic solvents, i.e., toluene, and n-heptane, using three DESs, i.e., reline, ethaline and glyceline. We employed a combination of experimental techniques such as densitometer, optical microscopy and FTIR, and MD simulations to characterize pure DESs and observe the extent of separation of asphaltenes in different combinations of solvent and DESs. The optical microscopy images show a distinct separation of asphaltene in n-heptane, with S1 performing the best at low concentrations of 0.1 mL. The optical images of DESs in the toluene - asphaltene solution also suggest a satisfactory aggregation, with S2 forming the highest concentration of aggregates. Further, we observed the formation of partial gel-type aggregates in the DES phase. The results of FTIR spectroscopy highlight the changes in functional groups of asphaltene - solvent - DES systems as compared to their pure constituents. Importantly, an increase in peak intensities is attributed to the presence of aggregates in the DES phase. MD simulations support the experimental observations in quantifying the aggregation and separation of the asphaltenes from the toluene/n-heptane in the presence of DESs. A slightly lower end-to-end distance and persistence length of asphaltene was observed for n-heptane, indicating that the asphaltenes were stable, implying better aggregation characteristics than toluene. The diffusion coefficient of asphaltene was lowest in the n-heptane - reline mixture compared to the toluene - glyceline/reline mixture due to the maximum separation of asphaltene from n-heptane. These observations were further validated by the trajectory density contours, which showed the formation of large and localized asphaltene aggregates in the presence of the DES in n-heptane and delocalized aggregates in toluene-based systems. The density contours of asphaltene - n-heptane - S1/S2 showed the formation of the smallest and densest clusters than those in S3, indicating maximum aggregation and separation, which agree with our experimental observations.

Overall, we observed that all three DESs were able to precipitate and eventually separate asphaltene that was dissolved in toluene, with

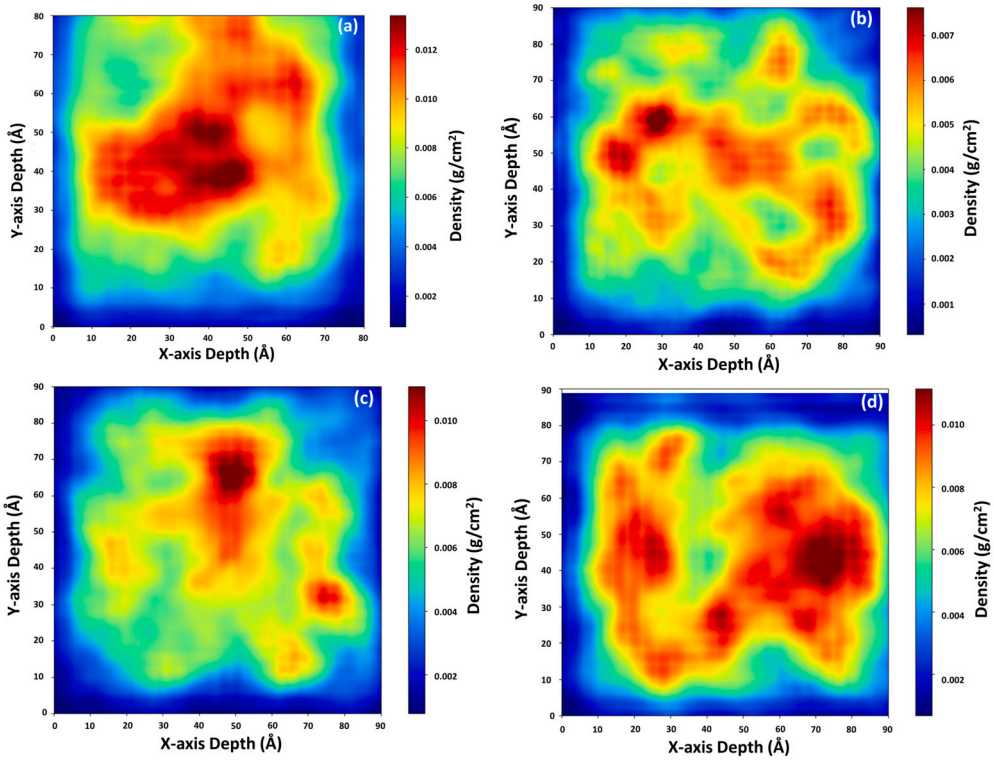

Fig. 11. The trajectory density contours for (a) asphaltene in pure toluene, (b) asphaltene in toluene- S1 DES, (c) asphaltene in toluene-S2 DES, (d) asphaltene in toluene-S3 DES are shown in the figure. Dark red colour denotes the maximum trajectory density (in g/cm^2), whereas the dark blue colour denotes the minimum trajectory density (in g/cm^2).

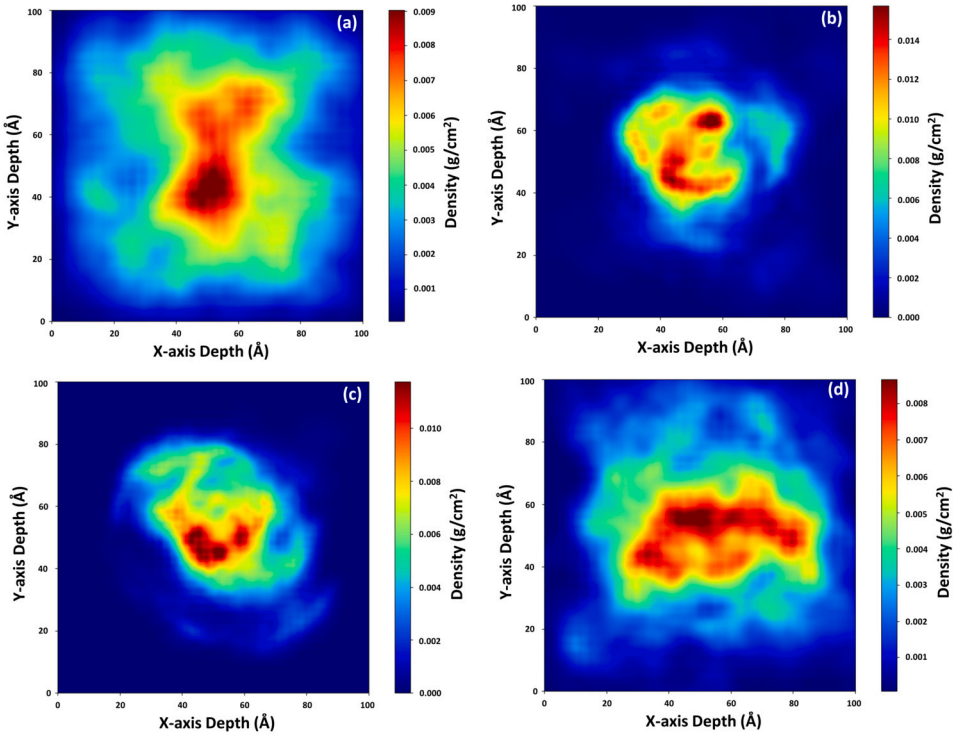

Fig. 12. The trajectory density contours for (a) asphaltene in pure n-heptane, (b) asphaltene in n-heptane- S1 DES, (c) asphaltene in n-heptane-S2 DES, (d) asphaltene in n-heptane-S3 DES are shown in the figure. Dark red colour denotes the maximum trajectory density (in g/cm^2), whereas the dark blue colour denotes the minimum trajectory density (in g/cm^2).

glyceline inducing maximum aggregation compared to reline and ethaline. Aliphatic organics like n-heptane have an opposing effect on the solubility of asphaltenes compared to toluene. Asphaltenes were spontaneously separated into the DES phase upon the addition of volumes as low as 0.1 mL in n-heptane, with reline causing maximum separation, evident from the saturation of aggregated asphaltenes in DES phase. Changes in the HBD and DES volumes, thus have a profound effect on the extent of asphaltene separation from aliphatic and aromatic organic solvents.

CRediT authorship contribution statement

Akshatha Hebbar: Investigation, Software, Validation, Visualization. **Devangshi Debraj:** Investigation, Validation, Visualization. **Sriprasad Acharya:** Conceptualization, Investigation, Supervision, Validation. **Sampath Kumar Puttapati:** Formal analysis, Resources, Validation. **Anoop Kishore Vatti:** Conceptualization, Investigation, Methodology, Software, Writing – original draft, Writing – review & editing. **Poulumi Dey:** Conceptualization, Methodology, Writing – original draft, Writing – review & editing.

Declaration of competing interest

The authors declare that they have no known competing financial interests or personal relationships that could have appeared to influence the work reported in this paper.

Data availability

Data will be made available on request.

Acknowledgements

AKV would like to thank Schrödinger Centre for Molecular Simulations, MAHE, Manipal. AKV and SA would like to thank Prof. Bharath Raj Guru for Optical Microscopy Facility.

References

[1] T.F. Yen, Asphaltenes, Springer US, Boston, MA, 1998, pp. 1–20.
[2] E.Y. Sheu, Petroleum asphalteneproperties, characterization, and issues, Energy Fuels 16 (1) (2002) 74–82, https://doi.org/10.1021/ef010160b.
[3] L.K. Kundarapu, S. Choudhury, S. Acharya, A.K. Vatti, S. Pandiyan, S. Gadag, U.Y. Nayak, P. Dey, Combined experimental and molecular dynamics investigation of 1d rod-like asphaltene aggregation in toluene-hexane mixture, J. Mol. Liq. 339 (2021) 116812, https://www.sciencedirect.com/science/article/pii/S0167732221015361.
[4] C. Pierre, L. Barré, A. Pina, M. Moan, Composition and heavy oil rheology, Oil and Gas Science and Technology, revue De L Institut Francais Du Petrole, Oil Gas Sci. Technol. 59 (2004) 489–501.
[5] K. Akbarzadeh, A. Hammami, A. Kharrat, D. Zhang, S. Allenson, J. Creek, S. Kabir, A. Jamaluddin, A.G. Marshall, R.P. Rodgers, et al., Asphaltenes problematic but rich in potential, Oilfield Rev. 19 (2) (2007) 22–43.
[6] E.Y. Sheu, O.C. Mullins, Asphaltenes, Springer, New York, NY, 1995.
[7] A. Saniere, I. Henaut, J.F. Argillier, Pipeline transportation of heavy oils, a strategic, economic and technological challenge, Oil Gas Sci. Technol. - Rev. IFP 59 (5) (2004) 455–466, https://doi.org/10.2516/ogst:2004031.
[8] I. Merdrignac, D. Espinat, Physicochemical characterization of petroleum fractions: the state of the art, Oil Gas Sci. Technol. - Revue de l'IFP 62 (2007) 7–32.
[9] L. Balestrin, W. Loh, Recent developments on the elucidation of colloidal aspects of asphaltenes and their relevance to oilfield problems, J. Braz. Chem. Soc. 31 (2020) 230–243.
[10] A. Sanati, M. Malayeri, O. Busse, J. Weigand, Utilization of ionic liquids and deep eutectic solvents in oil operations: progress and challenges, J. Mol. Liq. 361 (2022) 119641, https://www.sciencedirect.com/science/article/pii/S0167732222011795.
[11] O.C. Mullins, H. Sabbah, J. Eyssautier, A.E. Pomerantz, L. Barre, A.B. Andrews, Y. Ruiz-Morales, F. Mostowfi, R. McFarlane, L. Goual, R. Lepkowicz, T. Cooper, J. Orbulescu, R.M. Leblanc, J. Edwards, R.N. Zare, Advances in asphaltene science and the Yen-Mullins model, Energy Fuels 26 (7) (2012) 3986–4003, https://doi.org/10.1021/ef300185p.
[12] M. Porto, R. Angelico, P. Caputo, A.A. Abe, B. Teltayev, C.O. Rossi, The structure of bitumen: conceptual models and experimental evidences, Materials 15 (3), https://www.mdpi.com/1996-1944/15/3/905.
[13] T.F. Headen, E.S. Boek, N.T. Skipper, Evidence for asphaltene nanoaggregation in toluene and heptane from molecular dynamics simulations, Energy Fuels 23 (3) (2009) 1220–1229, https://doi.org/10.1021/ef800872g.
[14] J. Eyssautier, P. Levitz, D. Espinat, J. Jestin, J. Gummel, I. Grillo, L. Barré, Insight into asphaltene nanoaggregate structure inferred by small angle neutron and x-ray scattering, J. Phys. Chem. B 115 (21) (2011) 6827–6837, https://doi.org/10.1021/jp111468d, pMID: 21553910.
[15] A. Sanati, M. Malayeri, O. Busse, J. Weigand, Inhibition of asphaltene precipitation using hydrophobic deep eutectic solvents and ionic liquid, J. Mol. Liq. 334 (2021) 116100, https://www.sciencedirect.com/science/article/pii/S0167732221008278.
[16] D.L. Mitchell, J.G. Speight, The solubility of asphaltenes in hydrocarbon solvents, Fuel 52 (2) (1973) 149–152, http://www.sciencedirect.com/science/article/pii/0016236173900409.
[17] S. Kashefi, A. Shahrabadi, S. Jahangiri, M.N. Lotfollahi, H. Bagherzadeh, Investigation of the performance of several chemical additives on inhibition of asphaltene precipitation, Energy Sources, Part A, Recovery Utilization Environ. Eff. 38 (24) (2016) 3647–3652, https://doi.org/10.1080/15567036.2016.1198847.
[18] S. Jahangiri, A. Shahrabadi, A. Heydari, S. Javadian, A.H. Nazemi, S.M. Jahangiri, Choline chloride/monoethylene glycol deep eutectic solvent as a new asphaltene precipitation inhibitor, Pet. Sci. Technol. 35 (19) (2017) 1896–1902, https://doi.org/10.1080/10916466.2017.1369116.
[19] James H. Gary, Glenn E. Handwerk, Mark J. Kaiser, Petroleum Refining: Technology and Economics, 5 edition, CRC Press, 2007.
[20] A. Paiva, R. Craveiro, I. Aroso, M. Martins, R.L. Reis, A.R.C. Duarte, Natural deep eutectic solvents solvents for the 21st century, ACS Sustain. Chem. Eng. 2 (5) (2014) 1063–1071, https://doi.org/10.1021/sc500096j.
[21] T.F. Headen, E.S. Boek, Molecular dynamics simulations of asphaltene aggregation in supercritical carbon dioxide with and without limonene, Energy Fuels 25 (2) (2011) 503–508, https://doi.org/10.1021/ef1010397.
[22] Alternative Environmentally Friendly Solvents for Asphaltenes/Paraffins Removal from Oil Producing Wells, vol. Day 4 Thu, November 14, 2019 of Abu Dhabi International Petroleum Exhibition and Conference, d041S115R001, https://doi.org/10.2118/197697-MS.
[23] S.K. Singh, A.W. Savoy, Ionic liquids synthesis and applications: an overview, J. Mol. Liq. 297 (2020) 112038, https://www.sciencedirect.com/science/article/pii/S0167732219333719.
[24] H. Dong, Z. Wu, X. Li, X. Guo, J. Xu, Inhibition of asphaltene precipitation by ionic liquid polymers containing imidazole pendants and alkyl branches, Energy Fuels 36 (13) (2022) 6831–6842, https://doi.org/10.1021/acs.energyfuels.2c01021.
[25] C. Zheng, M. Brunner, H. Li, D. Zhang, R. Atkin, Dissolution and suspension of asphaltenes with ionic liquids, Fuel 238 (2019) 129–138, https://www.sciencedirect.com/science/article/pii/S0016236118317861.
[26] A.E. hoshoudy, A. Ghanem, S. Desouky, Imidazolium-based ionic liquids for asphaltene dispersion; experimental and computational studies, J. Mol. Liq. 324 (2021) 114698, https://www.sciencedirect.com/science/article/pii/S0167732220369403.
[27] A. Ghanem, R.D. Alharthy, S.M. Desouky, R.A. El-Nagar, Synthesis and characterization of imidazolium-based ionic liquids and evaluating their performance as asphaltene dispersants, Materials 15 (4), https://www.mdpi.com/1996-1944/15/4/1600.
[28] A.S. Ogunlaja, E. Hosten, Z.R. Tshentu, Dispersion of asphaltenes in petroleum with ionic liquids: evaluation of molecular interactions in the binary mixture, Ind. Eng. Chem. Res. 53 (48) (2014) 18390–18401, https://doi.org/10.1021/ie502672q.
[29] M. Boukherissa, F. Mutelet, A. Modarressi, A. Dicko, D. Dafri, M. Rogalski, Ionic liquids as dispersants of petroleum asphaltenes, Energy Fuels 23 (5) (2009) 2557–2564, https://doi.org/10.1021/ef800629k.
[30] S. Baghersaei, B. Mokhtari, N. Pourreza, B. Soltani Soulgani, Tetraalkylammonium and phosphonium salt for asphaltene dispersion; experimental studies on interaction mechanisms, Egypt. J. Petrol. 31 (3) (2022) 77–81, https://www.sciencedirect.com/science/article/pii/S1110062122000514.
[31] A.K. Vatti, P. Dey, S. Acharya, L.K. Kundarapu, S.K. Puttapati, Role of ionic liquid in asphaltene dissolution: a combined experimental and molecular dynamics study, Energy Fuels 36 (16) (2022) 9111–9120, https://doi.org/10.1021/acs.energyfuels.2c02076.
[32] L.G. Celia Silva, R.N. Martins, A.J.P. Carvalho, J.P.P. Ramalho, P. Morgado, E.J. Filipe, L.F. Martins, Influence of ionic liquids on the aggregation and pre-aggregation phenomena of asphaltenes in model solvent mixtures by molecular dynamics simulations and quantum mechanical calculations, Energy Fuels 36 (16) (2022) 9048–9065, https://doi.org/10.1021/acs.energyfuels.2c01387.
[33] J. Płotka-Wasylka, M. de la Guardia, V. Andruch, M. Vilková, Deep eutectic solvents vs ionic liquids: similarities and differences, Microchem. J. 159 (2020) 105539, https://www.sciencedirect.com/science/article/pii/S0026265X20322207.
[34] A.P. Abbott, D. Boothby, G. Capper, D.L. Davies, R.K. Rasheed, Deep eutectic solvents formed between choline chloride and carboxylic acids: versatile alternatives to ionic liquids, J. Am. Chem. Soc. 126 (29) (2004) 9142–9147, https://doi.org/10.1021/ja048266j, pMID: 15264850.
[35] E.L. Smith, A.P. Abbott, K.S. Ryder, Deep eutectic solvents (dess) and their applications, Chem. Rev. 114 (21) (2014) 11060–11082, https://doi.org/10.1021/cr300162p, pMID: 25300631.
[36] Q. Zhang, K. De Oliveira Vigier, S. Royer, F. Jerome, Deep eutectic solvents: syntheses, properties and applications, Chem. Soc. Rev. 41 (2012) 7108–7146, https://doi.org/10.1039/C2CS35178A.

[37] C. Florindo, F.S. Oliveira, L.P.N. Rebelo, A.M. Fernandes, I.M. Marrucho, Insights into the synthesis and properties of deep eutectic solvents based on cholinium chloride and carboxylic acids, ACS Sustain. Chem. Eng. 2 (10) (2014) 2416–2425, https://doi.org/10.1021/sc500439w.

[38] M. Zhang, R. Tian, H. Han, K. Wu, B. Wang, Y. Liu, Y. Zhu, H. Lu, B. Liang, Preparation strategy and stability of deep eutectic solvents: a case study based on choline chloride-carboxylic acid, J. Clean. Prod. 345 (2022) 131028, https://www.sciencedirect.com/science/article/pii/S095965262200662X.

[39] Zhen Zhang, Xingyi Liu, Dong Yao, Zhaoyuan Ma, Jiangang Zhao, Wanxiang Zhang, Peizhe Cui, Yixin Ma, Zhaoyou Zhu, Yinglong Wang, Molecular kinetic extraction mechanism analysis of 1-butanol from n-heptane-1-butanol by choline-based DESs as extractants, J. Mol. Liq. 322 (2021) 114665, https://www.sciencedirect.com/science/article/pii/S0167732220369075.

[40] Jiafu Xing, Yajuan Qu, Zihao Su, Mengjin Zhou, Chao Sun, Yinglong Wang, Peizhe Cui, Phase equilibria and mechanism insights into the separation of isopropyl acetate and methanol by deep eutectic solvents, Ind. Eng. Chem. Res. 61 (51) (2022) 18881–18893, https://doi.org/10.1021/acs.iecr.2c03488.

[41] Zihao Su, Yanli Zhang, Dingchao Fan, Peizhe Cui, Zhaoyou Zhu, Yinglong Wang, Liquid-liquid equilibrium experiment and mechanism analysis of menthol-based deep eutectic solvents extraction for separation of fuel additive tert-butanol, Environ. Res. 218 (2023) 115043, https://www.sciencedirect.com/science/article/pii/S0013935122023702.

[42] Jianguang Qi, Yajuan Qu, Mengjin Zhou, Zihao Su, Xiaoying Zhang, Ranran Wei, Ke Xue, Zhaoyou Zhu, Fanqing Meng, Yinglong Wang, Phase behavior and molecular insights on the separation of dimethyl carbonate and methanol azeotrope by extractive distillation using deep eutectic solvents, Sep. Purif. Technol. 305 (2023) 122489, https://www.sciencedirect.com/science/article/pii/S1383586622020457.

[43] t.M. Cui Peizhe, Xingyi Liu, Fei Zhao, Zhaoyou Zhu, Lei Wang, Yinglong Wang, Ind. Eng. Chem. Res. 59 (36) (2020) 16077–16087, https://doi.org/10.1021/acs.iecr.0c02794.

[44] A. Mohsenzadeh, Y. Al-Wahaibi, A. Jibril, R.A. Hajri, S. Shuwa, The novel use of deep eutectic solvents for enhancing heavy oil recovery, J. Pet. Sci. Eng. 130 (2015) 6–15, https://www.sciencedirect.com/science/article/pii/S0920410515001254.

[45] M. Atilhan, S. Aparicio, Molecular dynamics study on the use of deep eutectic solvents for enhanced oil recovery, J. Pet. Sci. Eng. 209 (2022) 109953, https://www.sciencedirect.com/science/article/pii/S0920410521015679.

[46] A. Sanati, M.R. Malayeri, M. Nategh, O. Busse, J.J. Weigand, Study of asphaltene deposition in the presence of a hydrophobic deep eutectic solvent using xdlvo theory, Energy Fuels 35 (24) (2021) 19953–19962, https://doi.org/10.1021/acs.energyfuels.1c02390.

[47] A. Sanati, M.R. Malayeri, Hydrophobic deep eutectic solvent and glycolipid biosurfactant as green asphaltene inhibitors: experimental and theoretical studies, Energy Fuels 35 (6) (2021) 4791–4802, https://doi.org/10.1021/acs.energyfuels.0c03922.

[48] N. Pulati, A. Lupinsky, B. Miller, P. Painter, Extraction of bitumen from oil sands using deep eutectic ionic liquid analogues, Energy Fuels 29 (8) (2015) 4927–4935, https://doi.org/10.1021/acs.energyfuels.5b01174.

[49] N. Pulati, T. Tighe, P. Painter, Bitumen–silica interactions in a deep eutectic ionic liquid analogue, Energy Fuels 30 (1) (2016) 249–255, https://doi.org/10.1021/acs.energyfuels.5b02375.

[50] C. Hu, S. Fu, L. Zhu, W. Dang, T. Zhang, Evaluation and prediction on the effect of ionic properties of solvent extraction performance of oily sludge using machine learning, Molecules 26 (24), https://www.mdpi.com/1420-3049/26/24/7551.

[51] T.F. Headen, E.S. Boek, G. Jackson, T.S. Totton, E.A. Muller, Simulation of asphaltene aggregation through molecular dynamics: insights and limitations, Energy Fuels 31 (2) (2017) 1108–1125, https://doi.org/10.1021/acs.energyfuels.6b02161.

[52] Ali Ghamartale, Nima Rezaei, Sohrab Zendehboudi, Alternation of asphaltene binding arrangement in the presence of chemical inhibitors: molecular dynamics simulation strategy, Fuel 336 (2023) 127001, https://www.sciencedirect.com/science/article/pii/S001623612203825X.

[53] A. Yadav, S. Pandey, Densities and viscosities of (choline chloride urea) deep eutectic solvent and its aqueous mixtures in the temperature range 293.15 k to 363.15 k, J. Chem. Eng. Data 59 (7) (2014) 2221–2229, https://doi.org/10.1021/je5001796.

[54] E.A. Crespo, J.M. Costa, A.M. Palma, B. Soares, M.C. Martin, J.J. Segovia, P.J. Carvalho, J.A. Coutinho, Thermodynamic characterization of deep eutectic solvents at high pressures, Fluid Phase Equilib. 500 (2019) 112249, https://www.sciencedirect.com/science/article/pii/S0378381219303024.

[55] S.L. Perkins, P. Painter, C.M. Colina, Experimental and computational studies of choline chloride-based deep eutectic solvents, J. Chem. Eng. Data 59 (11) (2014) 3652–3662, https://doi.org/10.1021/je500520h.

[56] A.T. Celebi, T.J.H. Vlugt, O.A. Moultos, Structural, thermodynamic, and transport properties of aqueous reline and ethaline solutions from molecular dynamics simulations, J. Phys. Chem. B 123 (51) (2019) 11014–11025, https://doi.org/10.1021/acs.jpcb.9b09729, pMID: 31794220.

[57] D. Shah, F.S. Mjalli, Effect of water on the thermo-physical properties of reline: an experimental and molecular simulation based approach, Phys. Chem. Chem. Phys. 16 (2014) 23900–23907, https://doi.org/10.1039/C4CP02600D.

[58] B. Gurkan, H. Squire, E. Pentzer, Metal-free deep eutectic solvents: preparation, physical properties, and significance, J. Phys. Chem. Lett. 10 (24) (2019) 7956–7964, https://doi.org/10.1021/acs.jpclett.9b01980, pMID: 31804088.

[59] W.E.M. Schermer, P.M.J. Melein, F.G.A. van den Berg, Simple techniques for evaluation of crude oil compatibility, Pet. Sci. Technol. 22 (7–8) (2004) 1045–1054, https://doi.org/10.1081/LFT-120038695.

[60] X. Li, Y. Guo, E.S. Boek, X. Guo, Experimental study on kinetics of asphaltene aggregation in a microcapillary, Energy Fuels 31 (9) (2017) 9006–9015, https://doi.org/10.1021/acs.energyfuels.7b01170.

[61] B.S. Soulgani, F. Reisi, F. Norouzi, Investigation into mechanisms and kinetics of asphaltene aggregation in toluene n-hexane mixtures, Pet. Sci. 17 (2020) 457–466.

[62] Haghbakhsh Reza, Sona Raeissi, Densities and volumetric properties of choline chloride urea deep eutectic solvent and methanol mixtures in the temperature range of 293.15 323.15 K, J. Chem. Thermodyn. 124 (2018) 10–20, https://www.sciencedirect.com/science/article/pii/S0021961418301459.

[63] A. Yadav, S. Trivedi, R. Rai, S. Pandey, Densities and dynamic viscosities of (choline chloride glycerol) deep eutectic solvent and its aqueous mixtures in the temperature range (283.15 363.15) k, Fluid Phase Equilib. 367 (2014) 135–142, https://www.sciencedirect.com/science/article/pii/S0378381214000533.

[64] F. Mjalli, O. Ahmed, Ethaline and glyceline binary eutectic mixtures: characteristics and intermolecular interactions, Asia-Pac. J. Chem. Eng. 12 (2) (2017) 313–320, https://onlinelibrary.wiley.com/doi/abs/10.1002/apj.2074.

[65] Yanxin Wang, Chunyan Ma, Chang Liu, Xiaohua Lu, Xin Feng, Xiaoyan Ji, Thermodynamic study of choline chloride-based deep eutectic solvents with water and methanol, J. Chem. Eng. Data 65 (5) (2020) 2446–2457, https://doi.org/10.1021/acs.jced.9b01113.

[66] Vira Agieienko, Richard Buchner, A comprehensive study of density, viscosity, and electrical conductivity of (choline chloride glycerol) deep eutectic solvent and its mixtures with dimethyl sulfoxide, J. Chem. Eng. Data 66 (1) (2021) 780–792, https://doi.org/10.1021/acs.jced.0c00869.

[67] Anita Yadav, Jyotsna Rani Kar, Maya Verma, Saeeda Naqvi, Siddharth Pandey, Densities of aqueous mixtures of (choline chloride+ethylene glycol) and (choline chloride+malonic acid) deep eutectic solvents in temperature range 283.15–363.15k, Thermochim. Acta 600 (2015) 95–101, https://www.sciencedirect.com/science/article/pii/S0040603114005449.

[68] B.B. Hansen, S. Spittle, B. Chen, D. Poe, Y. Zhang, J.M. Klein, A. Horton, L. Adhikari, T. Zelovich, B.W. Doherty, B. Gurkan, E.J. Maginn, A. Ragauskas, M. Dadmun, T.A. Zawodzinski, G.A. Baker, M.E. Tuckerman, R.F. Savinell, J.R. Sangoro, Deep eutectic solvents: a review of fundamentals and applications, Chem. Rev. 121 (3) (2021) 1232–1285, https://doi.org/10.1021/acs.chemrev.0c00385, pMID: 33315380.

[69] H. Groenzin, O.C. Mullins, Asphaltene molecular size and structure, J. Phys. Chem. A 103 (50) (1999) 11237–11245, https://doi.org/10.1021/jp992609w.

[70] Edo S. Boek, Dmitry S. Yakovlev, Thomas F. Headen, Quantitative molecular representation of asphaltenes and molecular dynamics simulation of their aggregation, Energy Fuels 23 (3) (2009) 1209–1219, https://doi.org/10.1021/ef800876b.

[71] Chao Lu, Chuanjie Wu, Delaram Ghoreishi, Wei Chen, Lingle Wang, Wolfgang Damm, Gregory A. Ross, Markus K. Dahlgren, Ellery Russell, Christopher D. Von Bargen, Robert Abel, Richard A. Friesner, Edward D. Harder, Opls4: improving force field accuracy on challenging regimes of chemical space, J. Chem. Theory Comput. 17 (7) (2021) 4291–4300, https://doi.org/10.1021/acs.jctc.1c00302, pMID: 34096718.

[72] K.J. Bowers, E. Chow, H. Xu, R.O. Dror, M.P. Eastwood, B.A. Gregersen, J.L. Klepeis, I. Kolossvary, M.A. Moraes, F.D. Sacerdoti, J.K. Salmon, Y. Shan, D.E. Shaw, Scalable algorithms for molecular dynamics simulations on commodity clusters, in: Proceedings of the 2006 ACM/IEEE Conference on Supercomputing, SC '06, ACM, New York, NY, USA, 2006, http://doi.acm.org/10.1145/1188455.1188544.

[73] Schrödinger release 2021-1, in: Schrödinger Release 2021-1, Desmond Molecular Dynamics System, D.E. Shaw Research, Schrödinger, LLC, New York NY, 2021.

[74] N. Haji-Akbari, P. Masirisuk, M.P. Hoepfner, H.S. Fogler, A unified model for aggregation of asphaltenes, Energy Fuels 27 (5) (2013) 2497–2505, https://doi.org/10.1021/ef4001665.

[75] M. Porto, R. Angelico, P. Caputo, A.A. Abe, B. Teltayev, C.O. Rossi, The structure of bitumen: conceptual models and experimental evidences, Materials 15 (3), https://www.mdpi.com/1996-1944/15/3/905.

[76] C.M. Sorensen, A. Chakrabarti, The sol to gel transition in irreversible particulate systems, Soft Matter 7 (2011) 2284–2296, https://doi.org/10.1039/C0SM00228C.

[77] T. Juric, D. Uka, B.B. Hollo, B. Jovic, B. Kordic, B.M. Popovic, Comprehensive physicochemical evaluation of choline chloride-based natural deep eutectic solvents, J. Mol. Liq. 343 (2021) 116968, https://www.sciencedirect.com/science/article/pii/S0167732221016925.

[78] R.K. Ibrahim, M. Hayyan, M.A. AlSaadi, S. Ibrahim, A. Hayyan, M.A. Hashim, Physical properties of ethylene glycol-based deep eutectic solvents, J. Mol. Liq. 276 (2019) 794–800, https://www.sciencedirect.com/science/article/pii/S0167732217303690.

[79] J.D. Cyran, A.T. Krummel, Probing structural features of self-assembled violanthrone-79 using two dimensional infrared spectroscopy, J. Chem. Phys. 142 (21) (2015) 212435, https://doi.org/10.1063/1.4919637.

[80] A.K. Vatti, A. Caratsch, S. Sarkar, L.K. Kundarapu, S. Gadag, U.Y. Nayak, P. Dey, Asphaltene aggregation in aqueous solution using different water models: a classical molecular dynamics study, ACS Omega 5 (27) (2020) 16530–16536, https://doi.org/10.1021/acsomega.0c01154, pMID: 32685817.

[81] J.N. Milstein, J.-C. Meiners, Worm-Like Chain, W.L.C. Model, Springer, Berlin Heidelberg, Berlin, Heidelberg, 2013, pp. 2757–2760.

[82] S. Brinkers, H.R.C. Dietrich, F.H. de Groote, I.T. Young, B. Rieger, The persistence length of double stranded dna determined using dark field tethered particle motion, J. Chem. Phys. 130 (21) (2009) 215105, https://doi.org/10.1063/1.3142699.
[83] Surabhi Aswath, Poulumi Dey, Anoop Kishore Vatti, Probing the effect of aliphatic ionic liquids on asphaltene aggregation using classical molecular dynamics simulations, ACS Omega 8 (18) (2023) 16186–16193, https://doi.org/10.1021/acsomega.3c00515.
[84] Understanding Molecular, Simulation: from algorithms to applications, in: D. Frenkel, B. Smit (Eds.), Understanding Molecular Simulation, second edition, Academic Press, San Diego, 2002.